A&A 518, A33 (2010)
DOI: 10.1051/0004-6361/201014400

Astronomy & Astrophysics

Radio polarimetry of 3C 119, 3C 318, and 3C 343 at milliarcsecond resolution

F. Mantovani[1], A. Rossetti[1], W. Junor[2], D. J. Saikia[3,4], and C. J. Salter[5]

[1] Istituto di Radioastronomia – INAF, via Gobetti 101, 40129 Bologna, Italy
e-mail: fmantovani@ira.inaf.it
[2] Los Alamos National Laboratory, Los Alamos, NM 87545, USA
[3] National Centre for Radio Astrophysics, TIFR, Post Bag 3, Ganeshkhind, Pune 411 007, India
[4] ICRAR, University of Western Australia, Crawley, WA 6009, Australia
[5] Arecibo Observatory, HC3 Box 53995, Arecibo, Puerto Rico 00612

Received 10 March 2010 / Accepted 4 May 2010

ABSTRACT

Aims. We report new Very Long Baseline Array (VLBA) polarimetric observations of the compact steep-spectrum (CSS) sources 3C 119, 3C 318, and 3C 343 at 5 and 8.4 GHz.
Methods. We analysed our VLBA observations and derived milliarcsecond-resolution images of the total intensity, polarisation, and rotation measure (*RM*) distributions.
Results. The CSS source 3C 119, associated with a possible quasar, has source rest-frame *RM* values up to ∼10 200 rad m^{-2} in a region that coincides with a change in the direction of the inner jet. This component is located ∼325 pc from the core, which is a variable source with a peaked radio spectrum. For 3C 318, which is associated with a galaxy, a rest-frame *RM* of ∼3030 rad m^{-2} was estimated for the brightest component contributing almost all of the polarised emission. Two more extended components were detected, that contain "wiggles" in the jet towards the southern side of the source. The CSS source 3C 343 contains two peaks of emission and a curved jet embedded in more diffuse emission. It exhibits complex field directions close to the emission peaks, which are indicative of rest-frame *RM* values in excess of ≈6000 rad m^{-2}. The locations of the cores in 3C 318 and 3C 343 are unclear.
Conclusions. The available data about mas-scale rest-frame *RM* estimates for CSS sources show that these have a wide range of values extending up to ∼40 000 rad m^{-2} in the central region of OQ172, and may be located at projected distances from the core of up to ∼1600 pc, as in 3C 43 where this feature has a rest-frame *RM* of ∼14 000 rad m^{-2}. The *RM* estimates for the cores of core-dominated radio sources indicate that in addition to responding to an overall density gradient of the magneto-ionic medium, geometry, orientation, and modes of fuelling may also play a significant role. In addition to these effects, the high values of *RM* in CSS sources are possibly caused by dense clouds of gas interacting with the radio jets. The observed distortions in the radio structures of many CSS sources are consistent with this interpretation.

Key words. polarization

1. Introduction

The number of compact steep-spectrum (CSS) sources with detailed polarimetric information available at milliarcsecond resolution remains small. Polarised radio emission from CSS radio galaxies is either very weak or below the detection limits at centimetre wavelengths. In contrast, CSS quasars have linear polarisation percentages of up to 10% above 1 GHz (Rossetti et al. 2008, and references therein). We have conducted a series of observations of CSS sources with significantly polarised emission and high values of rotation measure (*RM*) using the Very Long Baseline Array (VLBA).

The CSS objects are *young* radio sources with ages $<10^{3-5}$ yr. They have linear sizes ≤20 kpc[1] and steep high-frequency radio spectra ($\alpha > 0.5$; $S_\nu \propto \nu^{-\alpha}$). Being subgalactic in size, CSS sources reside deep within their host galaxies. Therefore, Faraday rotation effects are to be expected when their polarised synchrotron emission is observed through the host galaxy magneto-ionic interstellar medium (ISM). The comparison of polarised emission over a range of wavelengths is an important diagnostic of the physical conditions within and around these compact radio sources (see Cotton et al. 2003c, for an overview).

Existing subarcsec polarimetry has provided evidence in favour of the interaction of components of CSSs with dense clouds of gas, as seen for example in the CSS quasar 3C 147 (Junor et al. 1999).

Results for the first two CSS quasars observed in our ongoing program, B0548 + 165 and B1524 − 136, are available in Mantovani et al. (2002), while those for 3C 43 (B0127 + 233) are to be found in Mantovani et al. (2003). The results for 3C 147 (B0538 + 498) were presented by Rossetti et al. (2009). These sources have all been imaged with milliarcsecond resolution by means of full-Stokes VLBA observations.

In this paper, we report on multi-frequency VLBA, in addition to single Very Large Array (VLA) antenna, polarisation observations at 5 and 8.4 GHz for 3C 119 (B0429 + 415), 3C 318 (B1517 + 204), and 3C 343 (B1634 + 628).

In Sect. 2, we summarise the observations and data processing. Section 3 describes the new information obtained about the structural and polarisation properties of 3C 119, 3C 318, and 3C 343. Discussion and conclusions are presented in Sects. 4 and 5, respectively.

[1] $H_0 = 71$ km s^{-1} Mpc^{-1}, $\Omega_m = 0.27$, $\Omega_{vac} = 0.73$.

Table 1. VLBA+VLA1 observing parameters.

Sources	Obs. Date	Duration	Fringe finder	Polarisation calibrators
3C 119	05 Dec. 2001	12 h	DA 193	3C 84 3C 138, DA 193
3C 318	29 Sep. 2001	12 h	OQ 208	3C 279, 3C 380
3C 343	25 Oct. 2001	12 h	OQ 208	3C 345, 3C 380
IFs	MHz	Bandwidth	Array	
IF1	4619	16 MHz	VLBA+VLA1	
IF2	4657	16 MHz	VLBA	
IF3	4854	16 MHz	VLBA+VLA1	
IF4	5094	16 MHz	VLBA	
IF1–4	8421	64 MHz	VLBA+VLA1	

2. Observations and data reduction

Polarimetric observations of 3C 119, 3C 318, and 3C 343 using the VLBA and one VLA antenna were carried out at 5 and 8.4 GHz as detailed in Table 1. The data were recorded in both right- and left-circular polarisation in four 8-MHz bands. At 5 GHz, these bands were spread across the available bandwidth of ≈500 MHz, allowing us to obtain truly simultaneous, independent, polarisation images. Only two of the four sub-bands could make use of the VLA antenna in the array due to limitations in the available VLA 5 GHz system. To increase the sensitivity to polarised emission at 8.4 GHz, we chose to use contiguous IFs for this band.

The data were correlated with the National Radio Astronomy Observatory (NRAO) VLBA processor at Socorro and calibrated, imaged, and analysed using the AIPS package. The flux density and polarisation calibrations were performed following the procedure described in Rossetti et al. (2009) for the source 3C 147 observed using the same system setup. The flux density calibration uncertainty is ≈3%. The compact polarised sources DA 193, 3C 345, and 3C 380 were used to determine the instrumental polarisation ("D-term") using the AIPS task PCAL. The solution showed that the instrumental polarisation was typically about of the order of 1%.

3. Results

3.1. 3C 119

At different times, the radio source 3C 119 was optically identified as either a galaxy or a quasar, as noted by Fanti et al. (1990), who classified it as a quasar. Its light is dominated by its nucleus, which has a morphology more typical of CSS quasars (de Vries et al. 1997). It has a reasonably broad Hβ profile and we presently classify it as a possible quasar. It has $m_v = 20$ and $z = 1.023$ (Eracleous & Halpern 1994), so that 1 mas corresponds to 8.086 pc. A MERLIN polarimetric image of 3C 119 at 5 GHz was obtained by Lüdke et al. (1998), who studied a sample of CSS sources. At their resolution, it appears barely resolved. Lüdke et al. pointed out that it exhibits extremely rapid depolarisation between 8.4 and 5 GHz. This was confirmed by Mantovani et al. (2009), who detected polarised emission of 8.8 and 5.9 % at 10.45 and 8.35 GHz respectively, whereas at 4.85 GHz the polarisation was below the detection limit (∼110 mJy, corresponding to about 2.7%) of their Effelsberg 100-m telescope observations.

The first VLBI images of 3C 119 with resolutions ≤10 mas were acquired by Fanti et al. (1986) at 18 and 6 cm. They found at least four components embedded in a complex, spiral, filamentary structure suggesting that the low brightness emission was distributed in filaments surrounding the brighter components. Global VLBI observations at 18 cm were also performed by Nan et al. (1991a). These observations, combined with MERLIN data taken at the same time, confirmed the existence of the four components found by Fanti et al. (1986). These were labelled A, B, C, and D, by Nan et al. (1991a) and we adopt the same nomenclature here. An additional three, extended components of low surface brightness, E, F and G, were also found by Nan et al. (1991a). Together, these components account for 90% of the total flux density of the source.

VLBI polarimetry of 3C 119 was first performed by Nan et al. (1999) using the VLBA at three widely-separated frequencies in the 8.4 GHz band. The brightest jet component they found, component C, has a smooth rotation measure gradient of 2300 rad m^{-2} mas^{-1}, which is indicative of a collision between the VLBI jet and a dense interstellar cloud.

3C 119 is included in the MOJAVE (Lister & Homan 2009, Monitoring Of Jets in Active galactic nuclei with VLBA Experiments) monitoring project at 15.4 GHz. Four images from 2002, 2006, 2008, and 2009 are available in their data archive. At this frequency, components A, B, and C are detected, while the low brightness emission detected by Nan et al. (1991a), is completely resolved out.

Our total intensity image of 3C 119 at 4.8 GHz, compiled using all four *C*-band IFs, and the image at 8.4 GHz, are presented in Fig. 1. The source exhibits a core-jet structure with four of the seven components, (A–D), being detected. The three brightest components are not aligned, but lie along a jet contain "wiggles". Components B and C are surrounded by a "halo" of spots, reminiscent of the low brightness emission in which the jet itself is embedded.

Component A is almost point-like in the available VLBI images. Using its flux density estimates for almost the same epoch at frequencies from 1.6 to 15.4 GHz, we find a spectrum (see Fig. 2) typical of a giga-peaked spectrum (GPS) source with a peak flux density around 5 GHz. In Fig. 2, the flux density measurements at frequencies >4.5 GHz were taken over a narrow range of dates. The measurement at 1.6 GHz (Nan et al. 1991a) was adopted assuming negligible temporal variability at that frequency. Component A is not detected at 50 cm (Nan et al. 1991b) with an upper limit of ∼40 mJy, which is consistent with its inverted spectrum at low frequencies. We note that the flux density at 8.4 GHz for this component declined from 117 to 70 mJy between December 1994 (Nan et al. 1999) and December 2001 (present work). The observations performed by MOJAVE at 15.4 GHz also indicate that the flux densities rose from 45 mJy in October 2002 to 116 mJy in March 2006, 149 mJy in May 2008, and 173 mJy in July 2009. This component clearly appears to be a variable GPS source. Variability in a small fraction of GPS sources was found by Jauncey et al. (2003). Therefore, component A is almost certainly the core of 3C 119.

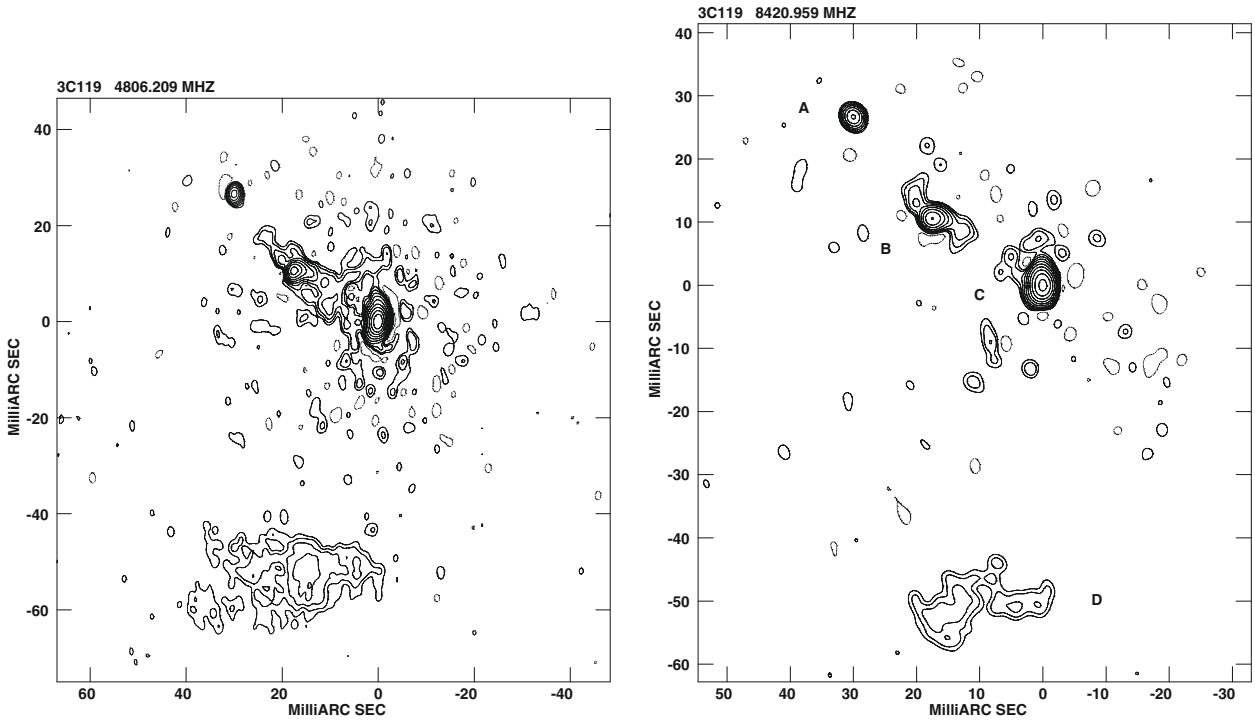

Fig. 1. (*Left*) The total intensity image of 3C 119 at 4.8 GHz made by combining all four *C*-band IFs, and (*right*) the total intensity 8.4 GHz image of 3C 119. The restoring beams are 2.25×1.57 mas^2 at -11.2°, and 2.04×1.83 mas^2 at 26.7°, respectively. The contour levels increase by factors of two from 1 mJy/beam for both images. Component designations are annotated on the 8.4 GHz image.

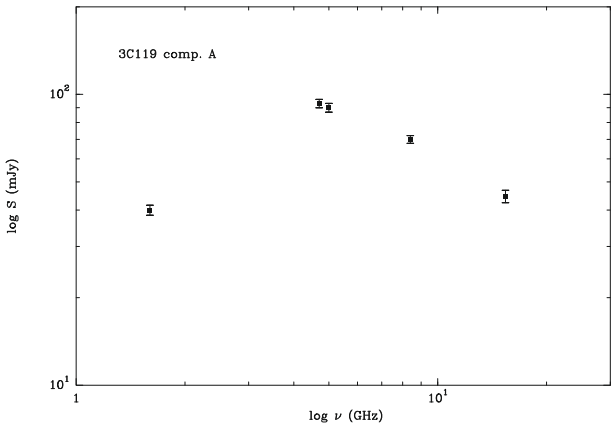

Fig. 2. Spectral index plot for component A made using flux density measurements taken almost at the same epoch for frequencies >4.5 GHz. The measurement at 1.6 GHz (Nan et al. 1991a) was adopted assuming negligible flux density variability at that frequency.

Mantovani et al. (2009) found total flux densities for 3C 119 of 4722 and 2677 mJy at 4.8 and 8.4 GHz, respectively, from their Effelsberg 100-m observations. The total flux density in our 4.8 GHz combined-IF image is 2838 mJy. At 8.4 GHz, we obtain 1531 mJy. The peak flux density is located in component C, being 987 and 660 mJy at 4.8 and 8.4 GHz, respectively.

3.1.1. Polarised emission from the inner jet of 3C 119

To compare the 5 and 8.4 GHz results, the images of 3C 119 were convolved to a resolution of 3.0×2.0 mas^2 at 0°. We detect polarised emission along the jet structure. However, components A and D show no or, at most, marginal, polarised emission above our detection limits at both 4.8 or 8.4 GHz. At *C*-band, we imaged the jet for each of the four individual IFs.

Figure 3 shows the total intensity and polarisation structure of the jet at *C*-band for the four individual IFs, while Fig. 4 shows the jet structure at *X*-band. The parameters derived from these images are listed in Table 2. Flux densities were determined using the AIPS task IMEAN on the same region of the *P* and *I* images. In Table 2, the total and peak flux densities, S, the rms noises, the polarised integrated flux densities, $S_{\rm pol}$ and its rms noise, the percentage polarisation, m, and the electric vector position angle (EVPA), χ, are listed for the four *C*-band IFs and *X*-band. For the core component A, which appears unresolved, we listed the values at the pixel of maximum total intensity.

Plots of χ against wavelength squared for components B and C are shown in Fig. 5. These were derived as follows. The median values and associated errors were computed for a box of five-by-five pixels around the peaks of polarised emission. At 15.4 GHz, the EVPA for both components was derived from the image made available by the MOJAVE archive from observations taken in 2002. These values have an accuracy of better than 5° (Lister & Homan 2005).

Both components show high values for the rotation measure. We derive $RM = 884$ rad m^{-2} (3618 rad m^{-2} in the source rest frame) for component B, whereas component C yields $RM = 1373$ rad m^{-2} (5620 rad m^{-2} in the source rest frame). We note that the EVPAs reported by Nan et al. (1999) for component C in the three sub-bands of their VLBA *X*-band observations are in close agreement with the linear fit in Fig. 5. They did not detect polarised emission in the region close to the peak of emission for component B, in contrast to our more sensitive observations. Polarised emission was detected by both sets of observations for the region immediately to the south west of compact component B, where almost the same values were found for the EVPAs.

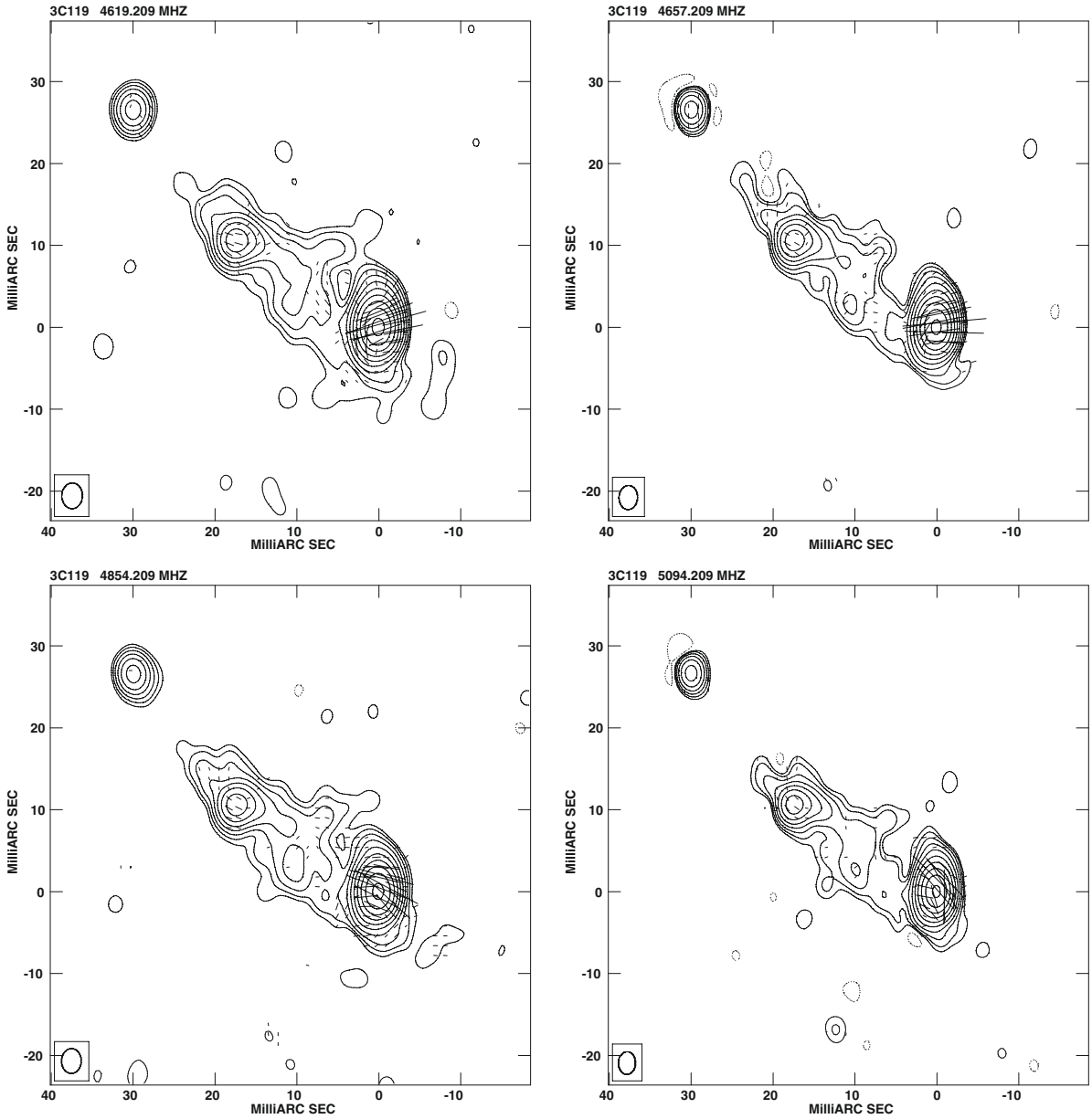

Fig. 3. The total intensity contours for 3C 119 A-C for the four *C*-band IFs with the polarisation ***E*** vectors superimposed. Contour levels increase by factors of two from 2 mJy/beam. A vector of 1 mas corresponds to 1.67 mJy/beam of polarised emission. The convolution beam is 3×2 mas^2 at PA 0°.

We have also plotted the distribution of *RM* around the emission peak in component C (Fig. 6). These plots were produced using the AIPS task RM, which requires EVPAs for up to four frequencies to compute the *RM* values. In this case, we selected frequencies of 4619, 4854, 5094, and 8421 MHz for which we have images available. Figure 6 shows that in a small area close to the peak of polarised emission, there are values of about 1400 rad m^{-2} (see Fig. 5). This area is surrounded by a region with much higher *RM*s lying in the range 2300 to 2500 rad m^{-2} (9400−10 200 rad m^{-2} in the source rest frame). This region coincides with a change in the direction of the inner jet of 3C 119. The value of *RM* reported for the integrated emission of 3C 119 by Mantovani et al. (2009) is 1928 rad m^{-2}. Clearly, C is the dominant component, strongly influencing the polarimetric parameters of the source.

Figure 6 (left) shows in grey scale the *RM* distribution for 3C 119 derived from the four frequencies (4619, 4854, 5094, and 8421 MHz) overlaid on the total-intensity contour image, while the panel on the right shows the *RM* contours. No redshift corrections were applied, so the *RM*s in the rest frame of the source will be higher by a factor of $(1 + z)^2 \approx 4$.

3.2. 3C 318

3C 318 is a radio galaxy at a redshift of 1.574 (1 mas = 8.554 pc). Single-dish observations of the object were recently made by Mantovani et al. (2009) who measured flux densities of 764 mJy at 4.8 GHz and 417 mJy at 8.4 GHz. The source is 3.4% and 6.6% polarised at 4.8 and 8.4 GHz, respectively. At lower frequencies, the polarisation drops below the detection limit of these Effelsberg observations. The *RM* derived by Mantovani et al. is 498 rad m^{-2}. Using the measurements of Tabara & Inoue (1980), we derive an *RM* of 342 rad m^{-2}. A similar value for the brightest component (420 rad m^{-2}) is reported

Table 2. Polarimetric parameters for the inner jet of 3C 119.

Comp. A IFs	MHz	S_{tot} mJy	S_{peak} mJy/b	rms(1σ) mJy/b	S_{pol} mJy	rms(1σ) mJy/b	m %	EVPA deg
IF1	4619	93.7	93.2	0.7	<0.6	0.11	<0.6	
IF2	4657	92.0	92.0	0.6	~0.9	0.11	~1	~0
IF3	4854	95.0	89.4	0.6	<0.6	0.12	<0.6	
IF4	5094	90.5	90.5	0.6	<0.7	0.13	<0.7	
IF1–4	8409	70.0	69.4	0.1		0.1		
Comp.B								
IF1	4619	251.3	216.3	0.7	1.7	0.11	0.7	73 ± 2
IF2	4657	267.2	207.1	0.6	1.4	0.11	0.5	62 ± 1
IF3	4854	272.0	211.2	0.6	1.8	0.12	0.7	59 ± 3
IF4	5094	273.8	199.2	0.6	1.6	0.13	0.6	44 ± 6
IF1–4	8409	155.6	134.2	0.1	0.8	0.09	0.5	−77 ± 5
Comp.C								
IF1	4619	1831.4	1255.7	0.7	19.6	0.11	1.1	105 ± 2
IF2	4657	1827.6	1204.3	0.6	24.2	0.11	1.3	92 ± 6
IF3	4854	1819.7	1229.1	0.6	24.3	0.12	1.3	62 ± 6
IF4	5094	1800.8	1157.2	0.6	22.1	0.13	1.2	40 ± 5
IF1–4	8409	1121.4	806.2	0.1	161.1	0.09	14.4	61 ± 2

Notes. The values for the three brightest components along the core-jet structure are organised as follows: Col. 1, IF number; 2, observing frequency; 3, total flux density; 4, peak flux density; 5, 1σ rms noise; 6, polarised flux density; 7, 1σ rms noise; 8, percentage polarisation; 9, electric vector position angle.

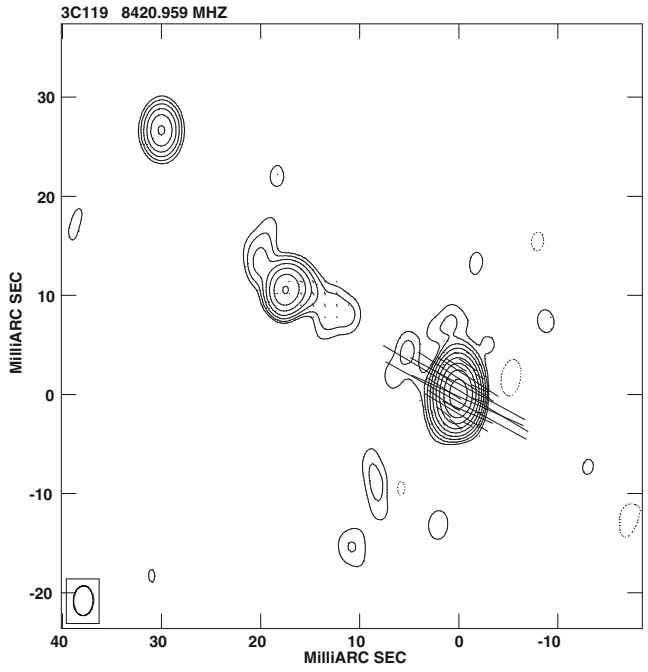

Fig. 4. The total intensity contours for 3C 119 A-C at *X*-band with the polarisation ***E*** vectors superimposed. Contour levels increase by factors of two from 2 mJy/beam. A vector of 1 mas corresponds to 6.7 mJy/beam of polarised emission. The convolution beam is 3×2 mas^2 at PA 0°.

by Taylor et al. (1992) from VLA observations with angular resolution of 0.4″. Taylor et al. found a polarisation percentage of ≈10% at 8.4 GHz.

A higher resolution *L*-band image of 3C 318 was obtained by Spencer et al. (1991) using combined MERLIN and EVN observations at a resolution of 35 × 33 mas^2. The component B detected by Akujor et al. (1991) with MERLIN at 5 GHz was resolved out, while the two northern components were found to show considerable structure and bright peaks. The total flux density detected by Akujor et al. (1991) was 543 mJy. Akujor & Garrington (1995) performed polarimetric observations of 3C 318 at 8.4 GHz with the VLA, and detected polarised emission (≈10%) mainly from the two northern components. VLA observations were also made by van Breugel et al. (1992) at 15 and 22 GHz. They found the northern region, in which the two components merge, to be 17% polarised. Additional polarimetric observations were performed by Lüdke et al. (1998) with MERLIN who found the brightest component to be 3.6% polarised at 5 GHz. In this image, 3C 318 shows a core-jet structure on one side and a lobe on the other. It is suggested that component K2 (Spencer et al. 1991) might be the core, although it appears resolved and does not have a flat spectrum.

In our 4.8 GHz VLBA observations, 3C 318 appears to be clearly resolved. Fringes were not detected at 8.4 GHz. Our 5 GHz image was made using the full bandwidth and, to be able to compare with previous VLBI observations, with a convolution beam of 35 × 33 mas^2 in PA 46° (Spencer et al. 1991). 3C 318 appears elongated in roughly the north south direction, the southern side contain a "wiggling" structure (Fig. 7). We follow the nomenclature of Spencer et al. (1991), who found four components named K1, K2, K3, and A. About 61% of the flux density found by Lüdke et al. (1998) is recovered here. The source parameters derived from our image are summarised in Table 3, the flux density values having been obtained using the AIPS task TVSTAT.

In our image, we find two other extended components, which we designate K4 and K5. These were not detected by the less sensitive observations of Spencer et al. (1991).

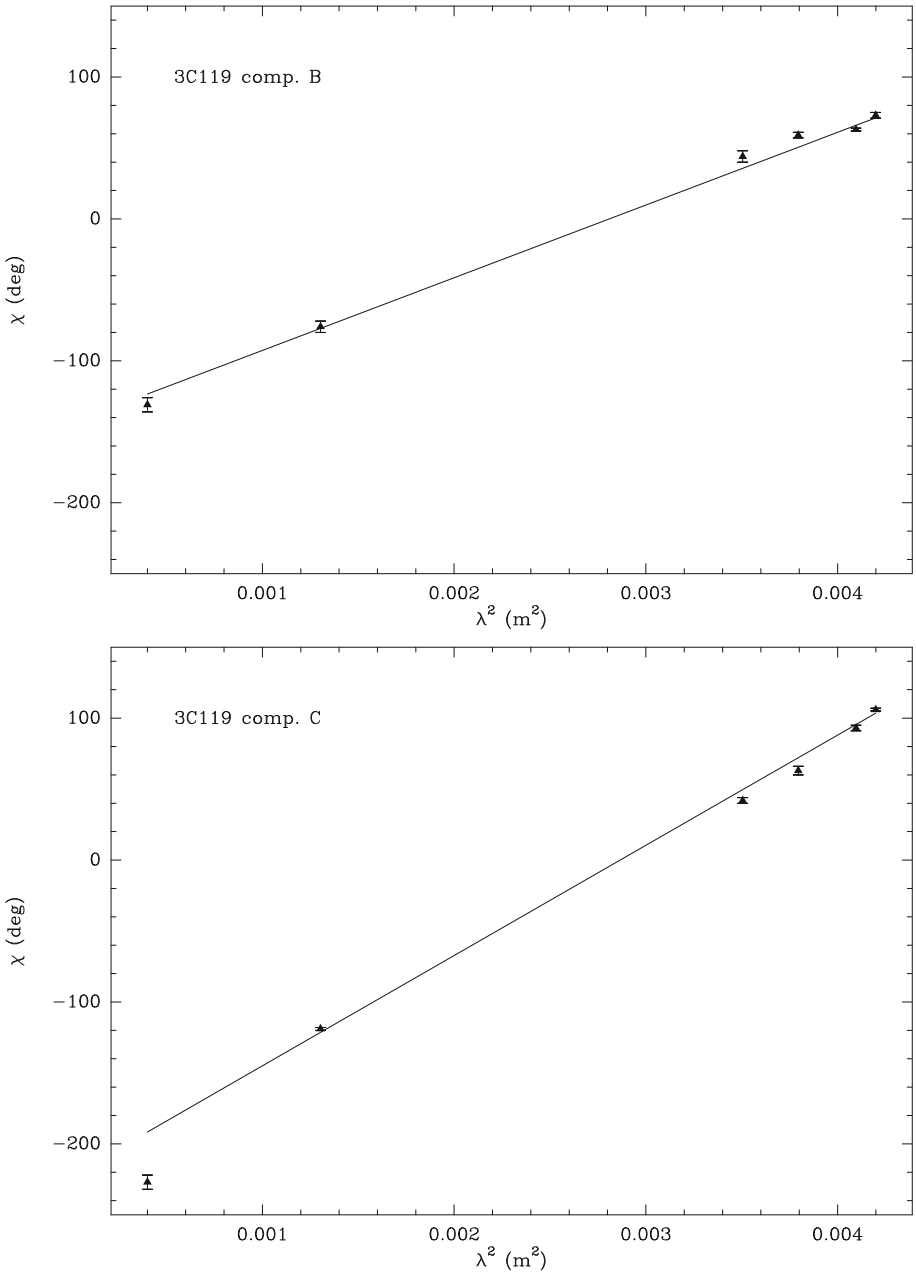

Fig. 5. Plots of the observed χ values for components B (*top*) and C (*bottom*) of 3C 119 as a function of λ^2 for the six available frequencies.

The brightest component, K2, is responsible for almost all of the polarised emission from 3C 318, and the magnetic field orientation appears to be almost constant over the region. A similar behaviour, but with different position angles, is presented by all available polarimetric images. Thus, we can derive the values of the rotation measure from these interferometric observations made at different frequencies. Values of the EVPA are taken from Lüdke et al. (1998) at 4996 MHz, Akujor & Garrington (1995) at 8414 MHz, Taylor et al. (1992) at 8515 MHz, and van Breugel et al. (1992) at 15 GHz, as well as from the present work, and are plotted in Fig. 8. The EVPA accuracies of these observations were not given, and values of $\pm 2^{\circ}$ have been assumed for both MERLIN and VLA EVPA determinations. The *RM* computed is $\approx$457 rad m^{-2}, not far from the values of 420 rad m^{-2} derived by Taylor et al. (1992), and 498 rad m^{-2} derived by Mantovani et al. (2009). We are again dealing with a CSS showing a very high *RM* of $\approx$3030 rad m^{-2} in the source rest frame at sub-arcsecond resolution.

3.3. 3C 343

3C 343 is associated with a quasar at $z = 0.988$ (1 mas = 8.017 pc). From their single dish observations, Mantovani et al. (2009) reported the detection of polarised flux density for this source only at 10.45 GHz at a level of 1.4%. A low level of polarised emission (0.8%) was also reported by Lüdke et al. (1998) from their MERLIN observations at 5 GHz in which the source appears barely resolved with a total flux density of 1434 mJy. Polarised emission is detected only in its eastern extension. Previous VLBI observations were performed by Fanti et al. (1985) and Nan et al. (1991b) at 1.6 GHz and 608 MHz, respectively. The mas structure of the source is quite peculiar, resembling a "fried egg".

Our total-intensity VLBA images of 3C 343 for the different *C*-band IFs are shown in Fig. 9, while the VLBA image at 8.4 GHz is shown in Fig. 10. The wide-band 5 GHz VLBA system allowed us to use four 8 MHz IF channels separated well

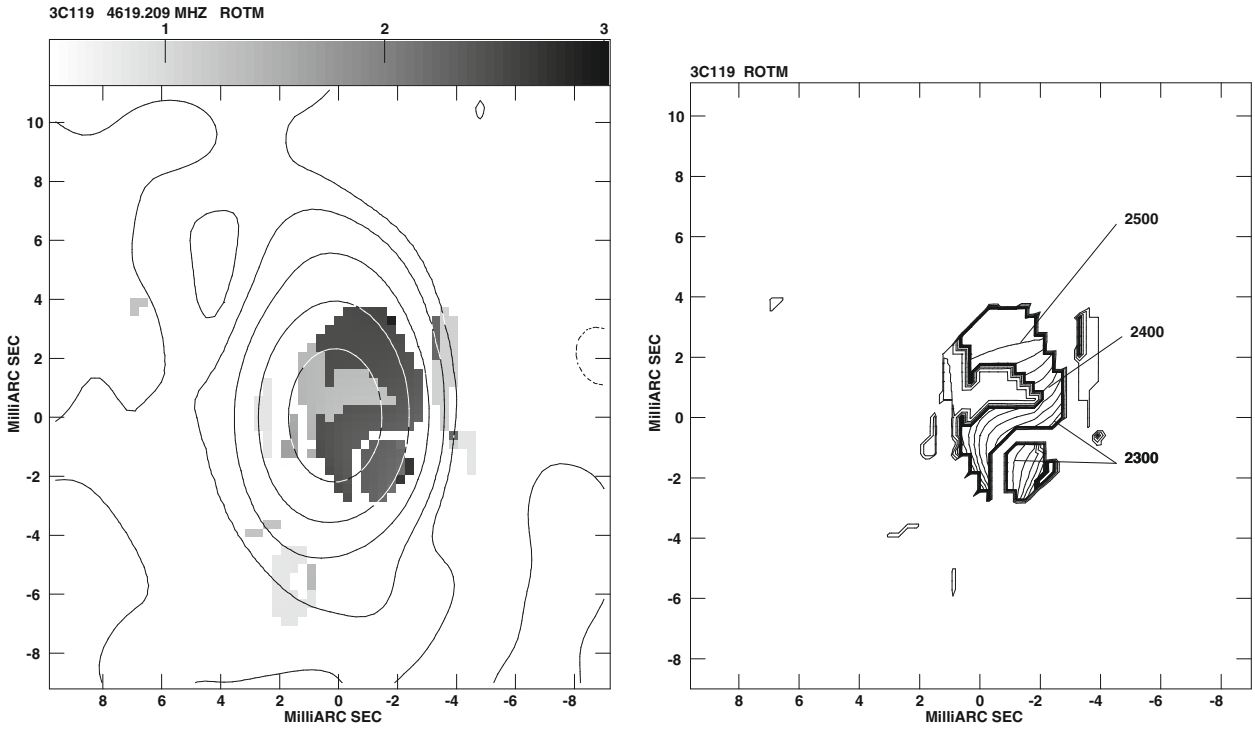

Fig. 6. The derived distribution of *RM* for 3C 119 C as a grey scale plot (*left*) and as a contour plot (*right*). The range of *RM* in the *left panel* is from 500 to 3000 rad m^{-2}, and the distribution is overlaid on the continuum image at 4619.2 MHz. The continuum contour levels are −2, 2, 8, 32, 128, and 512 mJy beam^{-1}. In the *right panel*, the *RM* contour levels are 100 × (10, 14, 18, 20, 22, 22.25, 22.50, 22.75, 23, 23.25, 23.50, 23.75, 24, 24.25, 24.50, 24.75, 25) rad m^{-2}.

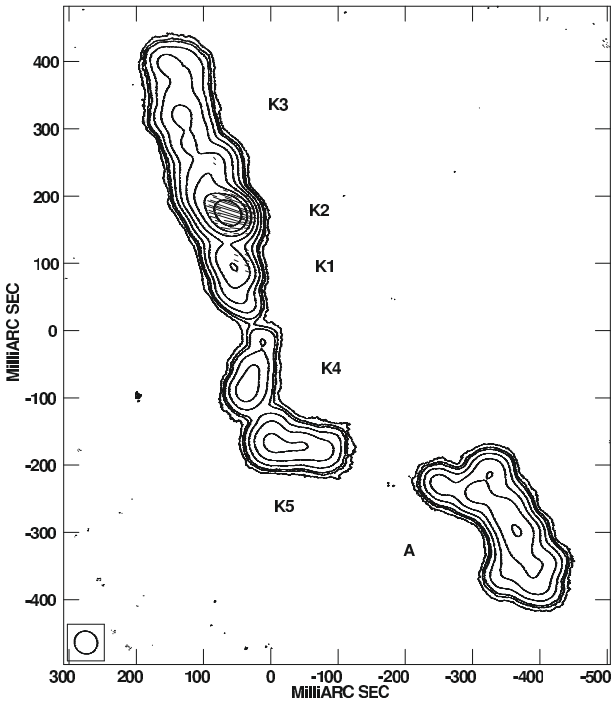

Fig. 7. The VLBA image of 3C 318 at 4.8 GHz. Contour levels are −0.35, 0.35, 0.7, 1, 2, 4, 8, 16, 32, 64, and 128 mJy/beam. A vector of 1 mas corresponds to 0.1 mJy/beam of polarised emission. The convolution beam is 35 × 33 mas^2 at PA 46°. The component designations are annotated on the image.

in frequency. Only *C*-band IFs 1 and 3 contain data from the VLA antenna which was included in the observing array. Two bright, compact components, A and B, are surrounded by weak,

Table 3. Parameters for 3C 318 at 4.8 GHz with a resolution of 35 × 33 mas^2 at 46°.

Comp.	$S_{\rm tot}$ mJy	$S_{\rm peak}$ mJy	$S_{\rm pol}$ mJy	m %	EVPA deg
K1	35.2	16.4	0.8	2.2	72 ± 5
K2	228.4	122.2	8.0	3.5	69 ± 5
K3	47.9	9.8			
K3	47.9	9.8			
K4	15.0	5.9			
K5	34.7	9.9			
A	107.5	16.8			

Notes. The rms noise (1σ) is 0.1 and 0.08 mJy/b for total and polarised flux density measurements, respectively.

diffuse emission. The two images made from data including the VLA antenna detected only diffuse emission, while the two images lacking baselines to the VLA antenna show the two prominent components, A and B, and the ridge of emission that resembles a curved radio jet. Both A and B have steep spectral indices between 4.8 and 8.4 GHz. The flux densities of these components were obtained with the AIPS task JMFIT, and component A (the eastern one) has $\alpha \approx 1.6$ (1.3 using the peak flux densities), while component B has $\alpha \approx 1.2$ (0.8 using the peak flux densities). Polarised emission is detected for both of these components and along the emission region between them. This all implies that either A or B is unlikely to be the core of 3C 343.

From the 8.4 GHz image, we note that a new compact component is clearly visible directly to the east of component A. This feature, which we label C in Fig. 10, is well separated from the brighter component A. Using the AIPS task JMFIT, we obtain total and peak flux densities of 7.7 and 3.5 mJy, respectively,

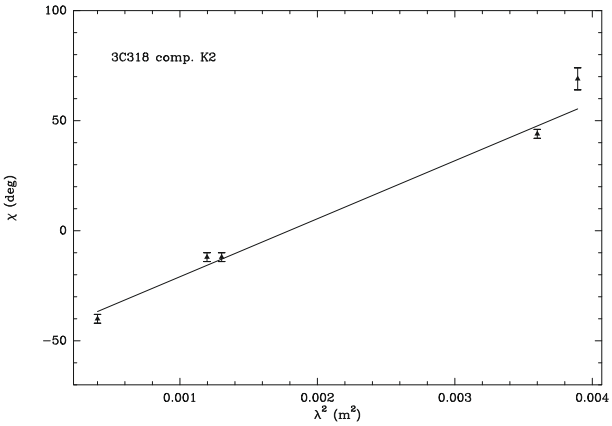

Fig. 8. A plot of the observed χ values for component K2 of 3C 318 as a function of λ^2 for the five available frequencies.

for component C. It is not detected in any of the *C*-band images of the same resolution, including that made by combining all four IFs to produce a 3σ upper limit peak flux density of 1 mJy. This corresponds to an inverted spectrum for C between 4.8 and 8.4 GHz, making it a candidate for being the core of 3C 343. Moreover, component C is situated nicely on the curved track of the jet as seen in Figs. 9b and d.

The parameters for components A and B are summarised in Table 4. The component peak and total flux densities, along with their deconvolved angular dimensions, were obtained using the AIPS task JMFIT. The degree of polarisation was estimated close to the peaks of emission in A and B. However, there appears to be large changes in the EVPAs close to the peaks of emission. Therefore, we have not quoted a single value in Table 4 but refer the reader to the distributions of EVPAs in Fig. 9.

The total flux density detected in a combined *C*-band image is 1274 mJy, about 89% of the flux density detected by MERLIN (Lüdke et al. 1998) and 85% of the flux density detected with the Effelsberg 100-m telescope by Mantovani et al. (2009). The polarisation percentage is estimated to be 0.96%, close to the value of 0.8% measured with MERLIN (Lüdke et al. 1998).

The total flux density detected in the VLBA image at 8.4 GHz (Fig. 10) is 553 mJy, 69% of the flux density detected by Mantovani et al. (2009). The polarised emission detected is 7.2 mJy, corresponding to 1.3%. The percentage polarisation drops by a factor of 0.73 between 8.4 and 4.8 GHz.

We detect polarised emission at all five observing frequencies. However, because of both the low level of polarisation and the lower sensitivity of the observations without the VLA antenna, mapping the *RM* distribution of 3C 343 is more difficult. It is clear from Fig. 9 that there may be changes of up to ∼90° in the orientation of the EVPAs close to the peaks of emission in components A and B. Significant polarisation is also not always detected from the same physical region of a component, possibly due to a combination of both varying sensitivity in the different IFs and varying *RM* across the source. These aspects have made it difficult to construct a reliable *RM* map. However, changes in the EVPAs between two neighbouring IFs, say IF2 and IF3, by of more than ∼30° in some regions are indicative of *RM* values higher than ∼1500 rad m^{-2} in the observer's frame. While more sensitive observations are required to produce a reliable *RM* map, a preliminary one using the present data seems to indicate similarly high values of *RM*.

4. Discussion

4.1. Comments on the three sources

The three CSSs we present here have mutually very different structures when imaged with mas resolution. The source 3C 119, which is associated with a possible quasar, has a complex shape when observed at low resolution, but has strong core-jet structure on resolutions of a few mas. We suggest that component A, which exhibits a convex spectrum, flux density variability, and either no, or at best marginal, polarisation above the detection limits, is the core. The jet contains "wiggles". From published images at sub-mas resolution, 3C 119 appears to maintain its collimation while presenting an overall spiral-like shape. Two bright, polarised blobs are seen along the jet. The brighter of these has a high rotation measure and strong depolarisation between 8.4 and 5 GHz, which we interpret as an indication of a strong interaction between the jet and a cloud in the ISM, possibly a dense narrow-line region (NLR) cloud. Although this interaction does not disrupt the jet, the jet does seem to change direction. The jet may also be bent close to our line of sight and move at apparent superluminal speed. We do not detect a counter-jet. The apparent speed of the two bright blobs (components B and C) along the approaching jet is most likely to be measured by the MOJAVE monitoring project, and this could possibly place constraints on the orientation of the ejection axis.

The source 3C 318 has an elongated jet with "wiggles" along its southern part. It is associated with a galaxy. Although the cores in quasars are often at the end of the jet, this need not be the case for a galaxy. In the present observations, we are unable to identify the exact core. Component K2, suggested by Spencer et al. (1991) to be the core, has a steep spectrum ($\alpha \approx 0.8$) and has a percentage polarisation of ≈3.4% at 4.8 GHz. It also has a high rotation measure, often visible in term of jets in CSS sources. This component is unlikely to be the radio core.

Among the three sources observed, 3C 343, which is associated with a quasar, presents the most unusual structure. The two brightest polarised components are embedded in a diffuse region of weak emission. It is unlikely that either is the core of the source. We propose that the component clearly visible to the east of component A in the *X*-band image, instead, is the possible core candidate. The *C*-band images without the VLA antenna do not detect the extended diffuse emission but show the two prominent components, A and B, and a ridge of emission that resembles a strongly curved jet.

The structures of all three CSS sources discussed in this paper exhibit large deviations from a collinear structure that are indicative of interactions of the jets with clouds in the interstellar medium of the host galaxy. Although two of the sources, 3C 119 and 3C 343, are associated with quasars, their cores are either weak or undetected, suggesting that projection effects caused by a small angle of inclination may not be important. However, jets may be bent towards the line of sight after collisions with clouds. Systematic monitoring of the knots or peaks of emission may help us to clarify whether this is indeed the case. The detection of high *RM*s towards the components in the radio jet/structure in both 3C 119 and 3C 343, as well as in 3C 318, supports the possibility of interaction of the jets with dense clouds. For an electron density of $\sim 10^3$ cm^{-3}, which is a reasonable estimate for the NLR clouds (e.g., Osterbrock 1989; Peterson 1997), and cloud sizes of ∼20 to 100 pc, the highest value of *RM* for 3C 119 yields magnetic field strengths in the range of ∼0.1 to 0.6 μG. The lower value of the cloud size was assumed to roughly correspond to the size of the radio components. The corresponding values of field strength for 3C 318 and 3C 343 are in the range

Table 4. Polarimetric parameters for the components A and B of 3C 343.

Comp. A IFs	MHz	S_{tot} mJy	S_{peak} mJy/b	rms(1σ) mJy/b	S_{pol} mJy	rms(1σ) mJy/b	maj.ax mas	min.ax. mas	PA deg	m %	EVPA deg
IF1	4619	102.1	30.3	0.4	3.7	0.2	16.8	8.4	108	3.6	see Fig. 9
IF2	4657	80.0	33.3	0.6	2.6	0.2	12.5	6.5	112	3.2	see Fig. 9
IF3	4854	80.3	33.5	0.3	4.8	0.2	11.9	7.1	113	6.0	see Fig. 9
IF4	5094	54.7	36.0	0.4	2.6	0.2	6.5	5.0	131	4.7	see Fig. 9
IF1–4	8409	33.0	16.3	0.2	1.6	0.1	8.7	7.5	105	4.8	-5 ± 3
Comp.B											
IF1	4619	470.5	77.2	0.4	2.7	0.2	19.4	16.7	117	0.6	see Fig. 9
IF2	4657	305.2	69.3	0.6	3.6	0.2	16.6	13.1	128	1.2	see Fig. 9
IF3	4854	391.9	80.6	0.3	4.3	0.2	16.8	14.7	149	1.1	see Fig. 9
IF4	5094	208.8	68.5	0.4	3.2	0.2	12.5	10.4	131	1.5	see Fig. 9
IF1–4	8409	198.7	51.4	0.2	5.9	0.1	15.8	11.8	5	3.0	-46 ± 1

Notes. The values for each components are organised as follows: Col. 1, IF number; 2, observing frequency; 3, total flux density; 4, peak flux density; 5, 1σ rms noise; 6, polarised flux density; 7, 1σ rms noise; 8, major axis; 9, minor axis; 10, major axis PA; 11, percentage polarisation; 12, electric vector position angle.

of ∼0.04−0.2 and 0.07−0.4 μG, respectively. These values are similar to those of, for example, Zavala & Taylor (2002). For a less dense medium with a thermal electron density of ∼1 cm^{-3} and a screen thickness of ∼1 kpc, as adopted by Mantovani et al. (2002), the magnetic field strenghts are in the range from ∼3.7 to 12.6 μG. These are similar to those estimated by Mantovani et al. (2002) for the CSS quasars B0548+165 and B1524−136, which also have high values of *RM* and bends in their radio structures.

4.2. A discussion of CSS quasars

To date, few CSSs have been imaged with polarimetric VLBI observations. Most of those that have are quasars. At present, 12 out of 24 quasars in the list of CSSs from the 3C and PW catalogues (Fanti et al. 1990) have published polarimetric VLBI data. Almost all of these show core-jet structures. Polarised emission is detected along the jets. Cores are usually weak and polarisation is not detected, in contrast to flat spectrum quasars. CSSs for which mas-scale values of *RM* have been derived are even rarer. Table 5 summarises parameters derived from existing observations. Except for 3C 287, whose low *RM* has been estimated from only two nearby frequencies, and 3C 286, which possibly has a low *RM* given its low integrated value but whose *RM* has not been determined with mas resolution, the remaining 12 sources have absolute rest-frame values of *RM* ranging from ∼1600 to 4×10^4 rad m^{-2}. In the case of OQ172, which also has the highest *RM*, the region of high *RM* is close to the core with the highest values occurring within ∼20 pc of the peak of emission in the core. This is also the case for the quasar 3C 309.1, which has a prominent radio core, the region of highest *RM* being situated in the vicinity of the radio core. For the remaining sources, the component of highest *RM* is distinct from the core, wherever a radio core could be identified. The distance from the core to the component with the highest *RM* varies from ∼37 to 1600 pc, the median separation being ∼400 pc. The regions of high *RM* are clearly within the NLR of the host galaxy.

The fractional polarisation usually tends to decrease with decreasing frequency. For the sources listed in Table 5, the components with the highest *RM* in 3C 119 and 3C 309.1 are strongly depolarised with DP values of ∼0.1 or less (beetween 5.0 and 8.4 GHz and 8.4 and 15 GHz respectively), while those in 3C 216 and OR−140 (B1524−136) exhibit hardly any depolarisation. While a high *RM* without depolarisation may be due to an external screen, a high *RM* along with depolarisation may be caused by unresolved structures in the screen and/or thermal plasma mixed with the radio-emitting material. Several examples of high *RM* with little or no significant depolarisation imply that the *RM* is due to a foreground Faraday screen, the NLR contributing to the observed *RM*. In all cases examined, a λ^2 law is closely followed over the observed frequency range. The jets are often distorted and this is interpreted in terms of jet-cloud interactions, although projection effects can also affect the observed structure if the jet is bent close to the line of sight. In many core-jet CSS quasars, high integrated Faraday rotation occurs where bends in the jet are found, suggesting that jet-cloud interactions play a significant role in the observed high *RM*s of these components. For example, amongst the 10 sources in Table 5 where a core or possible core has been identified, the highest values of *RM* occur at distances from the core ranging from ∼20 pc for OQ 172 to ∼1600 pc for 3C 43, excluding 3C 309.1 where the highest value is for the core. The median separation in the region of highest *RM* from the core is ∼300 pc. The axes of radio emission in these sources bend significantly after the region of highest *RM*. The PA of the latter differs from the axis defined by the core and the region of highest *RM* by ∼20 to 90°, the more extreme cases being 3C 43, 3C 119, 4C 16.14, and 3C 216. In the case of OQ 172, the region of highest *RM* is within ∼20 pc of the nucleus, and the jet shows a large deviation very close to the nucleus.

4.3. Comparison with pc-scale RMs in other AGNs

Apart from a few radio galaxies with either strong cores or jets, such as 3C 111, 3C 120, and M 87, most of the pc-scale *RM* estimates for other AGNs have been made for either core-dominated quasars or BL Lac objects. Early measurements with subarcsec resolution using the VLA inferred low core *RM*s at long wavelengths, the *RM*s increasing at shorter wavelengths as one probed deeper into the radio core (e.g., Saikia et al. 1998, and references therein). Subsequent mas-resolution observations with

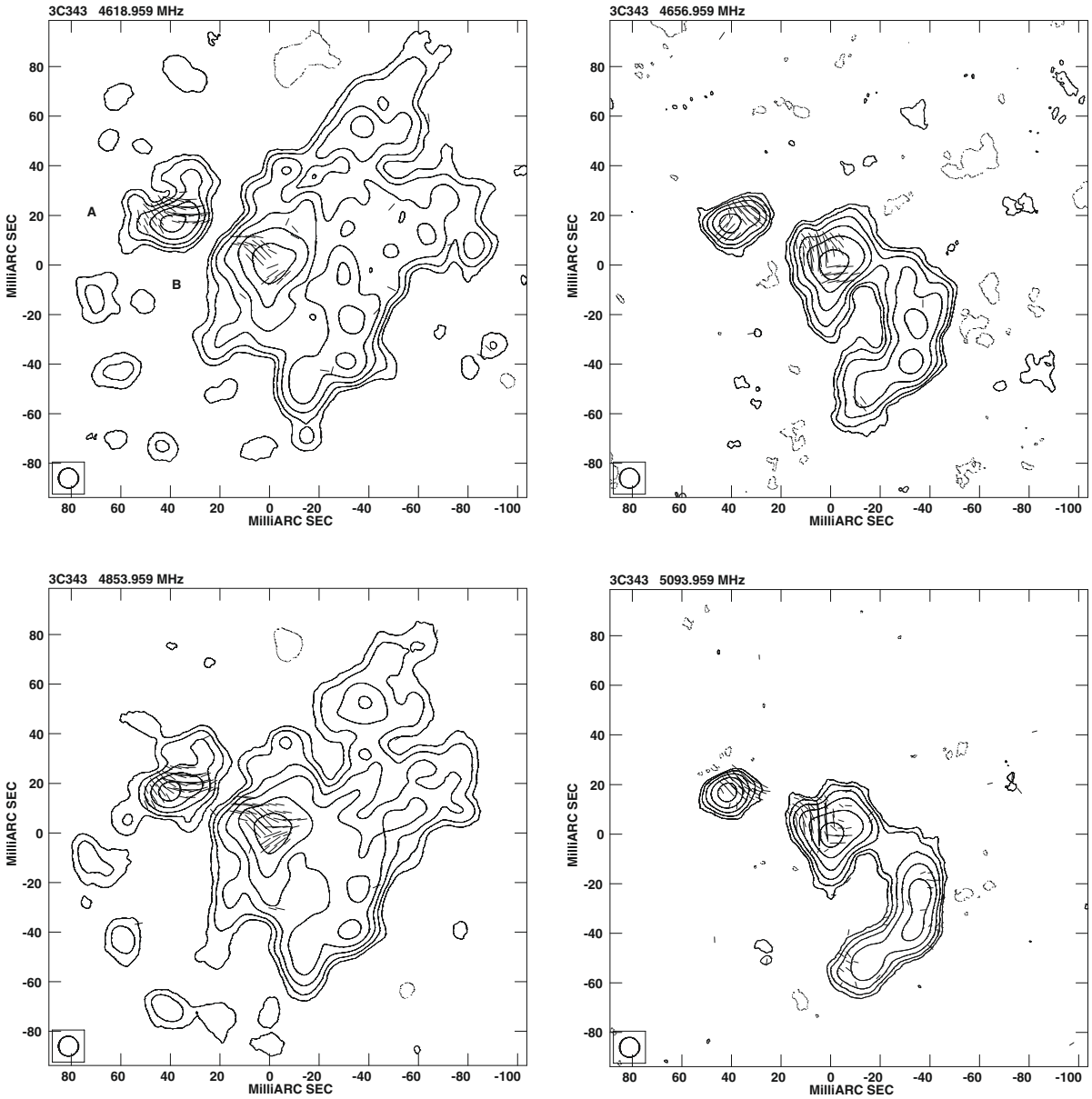

Fig. 9. The total intensity contours for 3C 343 A-C for the four *C*-band IFs with the ***E*** vectors superimposed. Contour levels increase by factors of two from 1.5 mJy/beam. A vector of 1 mas corresponds to 0.167 mJy/beam of polarised emission. The convolution beam is 8×8 mas^2.

the VLBA have revealed a wealth of information on core *RM*s (e.g., Zavala & Taylor 2002, 2003, 2004, and references therein; O'Sullivan & Gabuzda 2009, and references therein). A systematic study of the mas-scale *RM* properties of 40 quasars, radio galaxies, and BL Lac objects by Zavala & Taylor (2003, 2004) demostrated that the rest-frame core *RM* for quasars ranges up to $\sim 10^4$ rad m^{-2} with a median value of $\sim$1860 rad m^{-2} within $\sim$10 pc of the core. For BL Lac objects, their core *RM* values are usually within $\sim$1000 rad m^{-2} with a median value of $\sim$440 rad m^{-2}. The *RM*s of pc-scale jets decreases rapidly, the median values of the rest-frame *RM* for the jets being $\sim$460 and 260 rad m^{-2} for quasars and BL Lacs, respectively (Zavala & Taylor 2004). The few radio galaxies that have been studied exhibit evidence of moderate to high values of *RM*. For example, the core of 3C 111 is not significantly polarised, while the jet exhibits an *RM* of -750 rad m^{-2} 3 mas (2.8 pc) east of the core, decreasing further to -200 rad m^{-2} 5 mas (4.7 pc) east of the core. For 3C 120, while Zavala & Taylor (2002, 2003) estimate a core *RM* of 2080 rad m^{-2}, decreasing to $\sim$100 rad m^{-2} about 1 pc from the core, Gomez et al. (2008) find a localised region of high *RM* $\approx$3 to 4 mas (2–2.6 pc) from the core with a peak *RM* of $\sim$6000 rad m^{-2}. The *RM* values for M 87 could be determined from 18 to 27 mas ($\sim$1.5 to 2 pc) west of the core, and the values varied from ~ -5000 to 10^4 rad m^{-2} (Zavala & Taylor 2002, 2003). We noted that M 87 is in a cooling core cluster and that *RM* values as high as $\sim$8000 rad m^{-2} have been seen towards its 2-kpc radio lobes (Owen et al. 1990).

In comparison, the median value of *RM* for the CSS sources listed in Table 5 is $\sim$5000 rad m^{-2}, and values higher than $\sim$10 000 rad m^{-2} are seen to occur at distances from the core ranging from $\sim$300 to 1600 pc. This is quite unlike the regions of *RM* discussed earlier, almost all of which are very close to the radio core. For CSS objects, this implies the jets are often interacting with dense clouds of gas in the circumnuclear region of the host galaxy.

Table 5. Polarisation parameters of CSSs from mas-resolution observations.

Name	Alt. Name	z	Id.	m (%)	DP	$RM_{\rm rf}$ (rad m^{-2})	Notes	Ref.
3C 43	B0127+233	1.459	Q	$0.4_{1.6\,\rm GHz}$		14 236	E, ∼1600 pc from core	1
3C 119[a]	B0429+415	1.023	Q?	$14.4_{8.4\,\rm GHz}$	$0.08_{5.0/8.4}$	10 200	C, ∼325 pc from core	2
3C 138	B0518+165	0.759	Q	$3.6_{5.0\,\rm GHz}$		−5287	B1, ∼40 pc from core	3
3C 147	B0538+498	0.545	Q	$6.6_{8.4\,\rm GHz}$		−4872	BN, ∼37 pc from core A_0	4
4C 16.14[b]	B0548+165	0.474	Q	$6.2_{8.4\,\rm GHz}$	$0.26_{4.6/8.4}$	−4275	5C, ∼540 pc from core	5
3C 216	B0906+430	0.670	Q	$30.0_{8.4\,\rm GHz}$	$0.97_{4.8/8.4}$	2200	Arc, ∼1050 pc from core	6
3C 286[c]	B1328+307	0.849	Q	$11.0_{5.0\,\rm GHz}$			Core unclear	7,12
3C 287[d]	B1328+254	1.055	Q	$4.6_{5.0\,\rm GHz}$		∼0	Based on only 8.15 and 8.54 GHz	8
OQ 172[e]	B1442+101	3.529	Q	$2.7_{8.4\,\rm GHz}$		40 000	Within ∼20 pc from core	9,11
3C 309.1	B1458+718	0.905	Q	$1.5_{\ 15\,\rm GHz}$	$0.10_{8.4/15}$	−1633	Core *RM* between 8.4 and 15 GHz	10
3C 318	B1517+204	1.574	NG	$3.5_{4.8\,\rm GHz}$		3030	K2, Core unclear	2
OR−140[f]	B1524−136	1.687	Q	$30.2_{8.4\,\rm GHz}$	$\sim 1_{4.6-5.1/8.4}$	−10 000	C, ∼810 pc from core F	5
3C 343[g]	B1634+628	0.988	Q	$4.8_{8.4\,\rm GHz}$	$0.91_{4.6-5.1/8.4}$	>6000	core unclear	2
3C 454	B2249+185	1.757	Q	$10.9_{1.6\,\rm GHz}$		5334	B, ∼300 pc from possible core	1

Notes. Table 5 is organised as follows: Col. 1, source name; 2, alternative name; 3, redshift; 4, optical identification; 5, polarisation percentage of the emission; 6, highest value of depolarisation; 7, highest measured rest frame *RM*; 8, notes: letters refer to components designetion as in references quoted in Col. 9; 9, references: 1) Cotton et al. (2003); 2) present work; 3) Cotton et al. (2003b); 4) Rossetti et al. (2009); 5) Mantovani et al. (2002); 6) Venturi & Taylor (1999); 7) Jiang et al. (1996); 8) Dallacasa et al. (1998); 9) Udomprasert et al. (1997); 10) Aaron et al. (1997); 11) Mantovani, private communication; 12) Cotton et al. (1997).
[a] *m* and DP values are for component C, where the peak of polarised intensity is surrounded by a region with *RM* in the range of ∼9000−10 200 rad m^{-2}; [b] *m* and DP values are for the entire component 5; [c] fractional polarisations are 8.9 and 11.0% at 5 GHz for the western and eastern knots respectively (Cotton et al. 1997); polarisation is 11.3% for the dominant component with the VLA-A array at 4.885 GHz (Perley 1982); *RM* expected to be low but not determined with mas resolution; [d] polarisation is 4.6% with the VLA-A array at 4.885 GHz (Perley 1982); [e] polarisation is 2.0% with the VLA-A array at 4.885 GHz (Perley 1982); [f] DP estimated using 8.4 GHz and the mean of four measurements between 4.6 to 5.1 GHz; [g] DP estimated using 8.4 GHz and the mean of four measurements between 4.6 to 5.1 GHz for component A; there appears to be different regions of high *RM*.

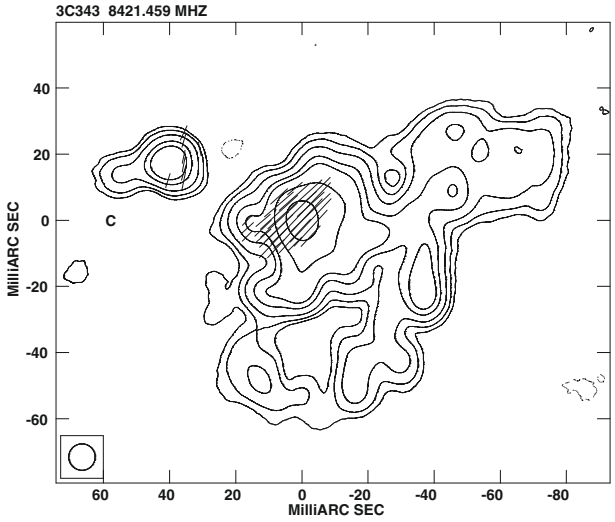

Fig. 10. The VLBA image of 3C 343 at 8.4 GHz using data from the full bandwidth. Contour levels increase by a factor of two from 0.75 mJy/beam. A vector of 1 mas corresponds to 0.1 mJy/beam of polarised emission. The convolution beam is 8×8 mas^2.

4.4. Environmental versus orientation effects

For quite some time, it has been apparent that the degree of core polarisation correlates with AGN classification. From subarcsec scale measurements with the VLA, it was pointed out quite early on that quasar cores tend to be more polarised than galaxy cores (Saikia et al. 1985, 1987). Milliarcsec-scale polarisation measurements also showed a similar trend, with the cores in BL Lac objects being slightly more polarised than the quasar cores (Cawthorne et al. 1993). Gabuzda et al. (1992) also demonstrated that the cores of BL Lacs are more polarised than quasars, a result also obtained for a larger sample of AGNs by Pollack et al. (2003). From arcsec-scale polarisation data, Saikia (1999) showed that BL Lac objects and core-dominated quasars had higher levels of core polarisation than lobe-dominated quasars and radio galaxies, and suggested that this might related to an orientation effect. Here, the low polarisation of the cores of radio galaxies, and perhaps the lobe-dominated quasars as well, were attributed by the authors to depolarisation by the obscuring torus. However, the observed degree of polarisation may also reflect the contribution of a small-scale jet, which may be more strongly polarised and contribute more significantly at smaller angles to the line of sight.

Taylor (2000) suggested that the *RM* values for BL Lac objects may be smaller than those of quasars, because their jets are believed to be inclined at smaller angles to the line of sight. This could arise if the relativistic jets cleared out the magneto-ionic material responsible for the Faraday rotation. Similar ideas were suggested by Saikia et al. (1998) to explain the low *RM* values for quasar cores determined from long-wavelength polarimetric observations with arcsec resolution. Although individual *RM* values in BL Lac objects are known to exceed thousands of rad m^{-2}, the median value of rest-frame *RM* for quasars is larger than that for the BL Lac objects by a factor of ∼4, consistent with the expectation of Taylor (2000). It appears that for quasars the long-wavelength measurements probe the outer regions of the nuclear jets on scales of tens of pc yielding low *RM* values as these are seen through regions that have been at least partially cleared of the magneto-ionic medium by the relativistic jets. Shorter wavelength observations with mas resolution probe deeper into the base of the jet, and yield high *RM*s indicating denser gas and/or higher magnetic fields than on the larger scales. It is relevant to note that O'Sullivan & Gabuzda (2009)

find the core *RM* to systematically increase with frequency, this being well described by a power law, providing information about the power law fall off of electron density and/or magnetic field with distance from the nucleus. In the scheme where orientation effects play a role, the cores of radio galaxies and any emission in their immediate vicinity would be expected to have high values of *RM* because of the effects of the obscuring torus.

An interesting characteristic of extragalactic radio sources is that there appear to be significant differences between the host galaxy and emission-line properties of Fanaroff-Riley class I and II sources (Fanaroff & Riley 1974), which may be related to the fuelling mechanism. While a significant fraction of high-luminosity radio sources have peculiar optical morphologies and high-excitation emission lines, reminiscent of gas-rich galaxy mergers, the low-luminosity radio sources do not share the same optical properties and have weak, low-excitation emission lines (Heckman et al. 1986; Baum et al. 1992, 1995). Hubble Space Telescope observations show that the low-power radio sources lack evidence of an obscuring torus and significant emission from a classical accretion disc (Chiaberge et al. 1999), and may be fuelled by quasi-spherical Bondi accretion of circum-galactic gas rather than gas-rich galaxy mergers (Hardcastle et al. 2007). The finding by Baldi & Capetti (2008) that high-excitation radio galaxies almost always show evidence of star formation, unlike their low-luminosity counterparts, is consistent with this trend. In our case, BL Lac objects are usually hosted by galaxies with low-excitation emission lines, while quasars are hosted in galaxies with high-excitation emission lines. This difference is also likely to affect the observed *RM*s of BL Lac objects and quasars, with the former expected to have smaller values.

For CSS sources, although orientation is also expected to play a role (e.g. Saikia et al. 1995), the cores are either weak or not clearly identified making it impossible to either determine their *RM*s or place robust limits on their degrees of polarisation. Amongst the sources listed in Table 5, the cores are strong enough for their *RM*s to be estimated in 3C 309.1 and OQ172, the values being ~ -1600 and 40 000 rad m^{-2}, respectively. While 3C 309.1 exhibits a large misalignment between the mas-scale and arcsec-scale structures, the jet in OQ 172 bends sharply west of the nucleus and the *RM* of the jet falls to less than 100 rad m^{-2} only 10 mas (~74 pc) from the nucleus (Udomprasert et al. 1997). Although the high values of *RM* may be partly due to these observations probing close to the nuclear region, the large bends in these sources imply that collisions with dense clouds of gas are also a significant factor. For the remaining CSS objects, where the regions of large *RM* occur at large distances from the nucleus, these large values are most likely to be caused by interactions of the jets with dense clouds of gas, some of which may also be fuelling the AGN activity.

5. Summary and conclusions

We have presented multi-frequency VLBA polarisation observations of three CSS sources, namely 3C 119, 3C 318, and 3C 343 to estimate their *RM* values. The radio source 3C 119 is associated with a possible quasar, and its *RM* in the source rest-frame has been found to be as high as ~10 200 rad m^{-2} in a region that coincides with a change in direction of the inner jet. This component is located at a projected distance of ~325 pc from the core, which is almost point-like, variable, has a peaked radio spectrum and is at best marginally polarised. The source 3C 318 is associated with a radio galaxy and its rest-frame *RM* has been found to reach a maximum of ~3030 rad m^{-2} for the brightest component, which contributes almost all of the polarised emission. These observations are more sensitive than those of Spencer et al. (1991) and have detected two more extended components, which trace "wiggles" in the jet towards the southern side of the source. Of the three, the CSS source 3C 343 has perhaps the most complex structure. It contains two peaks of emission and a curved jet embedded in more diffuse emission. It exhibits complex field directions near the peaks of emission, which indicate rest-frame *RM* values in excess of ≈4000 rad m^{-2}. The varying sensitivity of the different frequencies and the complex field patterns near the peaks of emission make it difficult to construct a reliable *RM* image for this source.

We have compiled the available data on mas-scale *RM* estimates for CSS sources. They exhibit a wide range of values with indications of a low *RM* for 3C 287 that needs to be confirmed from observations with a larger number of frequencies, to values as high as ≈40 000 rad m^{-2} in the central region of OQ172 (Udomprasert et al. 1997). The components with high *RM* may also occur at considerable distances from the core, e.g., in 3C 43 where the component with an *RM* of ~14 000 rad m^{-2} is located at a projected distance of ~1600 pc (Cotton et al. 2003a). The *RM* estimates for flat-spectrum cores in largely core-dominated radio sources appear to increase with frequency (see O'Sullivan & Gabuzda 2009), suggesting that as one probes deeper into the core or unresolved base of the jet, one samples regions of higher density and/or magnetic field in the magneto-ionic medium. On larger scales, the jet *RM*s tend to be low because these objects are observed along a line of sight where the magneto-ionic medium may have been swept out by the relativistic jets (e.g., Saikia et al. 1998; Taylor 2000; Zavala & Taylor 2004). The CSS objects for which *RM* values have been estimated are almost entirely quasars. While the effects of an overall density gradient in the magneto-ionic medium, along with effects of geometry, orientation, and modes of fuelling of the AGN, are likely to play a significant role, the high *RM* values in many of these CSS sources appear to be caused by dense clouds of gas interacting with the radio jets. They usually also exhibit large structural bends and distortions, consistent with the possibility of jet-cloud interactions in the interstellar medium of the host galaxy. Some of these gas clouds may also be responsible for fuelling the AGN activity.

Acknowledgements. We thank an anonymous referee for his/her very helpful comments and suggestions, and for a careful reading of the manuscript of this paper. The VLBA is operated by the U.S. National Radio Astronomy Observatory which is a facility of the National Science Foundation operated under a cooperative agreement by Associated Universities, Inc. This research has made use of data from the MOJAVE database that is maintained by the MOJAVE team (Lister et al. 2009, AJ, 137, 3718). This research has made use of the NASA/IPAC Extragalactic Database (NED) which is operated by the Jet Propulsion Laboratory, California Institute of Technology, under contract with the National Aeronautics and Space Administration. F.M. likes to thank Prof. Anton Zensus, Director, for the kind hospitality at the Max-Planck-Institut für Radioastronomie, Bonn, for a period during which part of this work has been done.

References

Aaron, S., Roberts, D. H., & Wardle, J. F. C. 1997, Vistas in Astr., 41, 225
Akujor, C. E., & Garrington, S. T. 1995, A&AS, 112, 235
Akujor, C. E., Spencer, R. E., Zhang, F. J., et al. 1991, MNRAS, 250, 215
Baldi, R. D., & Capetti, A. 2008, A&A, 489, 989
Baum, S. A., Heckman, T. M., & van Breugel, W. 1992, ApJ, 389, 208
Baum, S. A., Zirbel, E. L., & O'Dea, C. P. 1995, ApJ, 451, 88
Cawthorne, T. V., Wardle, J. F. C., Roberts, D. H., & Gabuzda, D. C. 1993, ApJ, 416, 519
Chiaberge, M., Capetti, A., & Celotti, A. 1999, A&A, 349, 77
Cotton, W. D., Fanti, C., Fanti, R., et al. 1997, A&A, 325, 479
Cotton, W. D., Spencer, R., Saikia, D. J., & Garrington, S. 2003a, A&A, 403, 537

Cotton, W. D., Dallacasa, D., Fanti, C., et al. 2003b, A&A, 406, 43
Cotton, W. D., Dallacasa, D., Fanti, C., et al. 2003c, PASA, 20, 12
Dallacasa, D., Schilizzi, R. T., & Nan Rendong 1998, ed. A. J. Zensus, G. B. Taylor, & J. M. Wrobel, IAU Colloq., 164, ASP Conf. Ser., 144, 117
de Vries, W. H., O'Dea, C. P., Baum, S. A., et al. 1997, ApJS, 110, 191
Eracleous, M., & Halpern, J. P. 1994, ApJS, 90,1
Fanaroff, B. L., & Riley, J. M. 1974, MNRAS, 167, 31P
Fanti, C., Fanti, R., Parma, P., et al. 1985, A&A, 143, 292
Fanti, C., Fanti, R., Schilizzi, R. T., et al. 1986, A&A, 170, 10
Fanti, R., Fanti, C., Schilizzi, R. T., et al. 1990, A&A, 231, 333
Gabuzda, D. C., Cawthorne, T. V., Roberts, D. H., & Wardle, J. F. C. 1992, ApJ, 388, 40
Gómez, J. L., Marscher, A. P., Jorstad, S. G., Agudo, I., & Roca-Sogorb, M. 2008, ApJ, 681, L69
Hardcastle, M. J., Evans, D. A., & Croston, J. H. 2007, MNRAS, 376, 1849
Heckman, T. M., Smith, E. P., Baum, S. A., et al. 1986, ApJ, 311, 526
Jauncey, D. L., King, E. A., Bignall, H. E., et al. 2003, PASA, 20, 151
Jiang, D. R., Dallacasa, D., Schilizzi, R. T., et al. 1996, A&A, 312, 380
Junor, W., Salter, C. J., Saikia, D. J., Mantovani, F., & Peck, A. B. 1999, MNRAS, 308, 955
Lister, M. L., & Homan, D. C. 2005, AJ, 130, 1389
Lister, M. L., Aller, H. D., Aller, M. F., et al. 2009, AJ, 137, 3718
Lüdke, E., Garrington, S. T., Spencer, R. E., et al. 1998, MNRAS, 299, 467
Mantovani, F., Junor, W., Ricci, R., Saikia, D. J., et al. 2002, A&A, 389, 58
Mantovani, F., Junor, W., Saikia, D. J., & Salter, C. 2003, PASA, 20, 123
Mantovani, F., Mack, K.-H., Montenegro-Montes, F. M., et al. 2009, A&A, 502, 61
Nan, R.-D., Schilizzi, R. T., van Breugel, W. J. M., et al.1991a, A&A, 245, 449
Nan, R. D., Schilizzi, R. T., Fanti, C., & Fanti, R. 1991b, A&A, 252, 513
Nan, R. D., Gabuzda, D. C., Kameno, S., et al. 1999, A&A, 344, 402
Osterbrock, D. E. 1989, Astrophysics of Gaseous Nebulae and Active Galactic Nuclei (Mill Valley: University Science Books)
O'Sullivan, S. P., & Gabuzda, D. C. 2009, MNRAS, 400, 26
Owen, F. N., Eilek, J. A., & Keel, W. C. 1990, ApJ, 362, 449
Perley, R. A. 1982, AJ, 87, 859
Peterson, B. M. 1997, An introduction to Active Galactic Nuclei (Cambridge: Cambridge University Press)
Pollack, L. K., Taylor, G. B., & Zavala, R. T. 2003, ApJ, 589, 733
Rossetti, A., Dallacasa, D., Fanti, C., et al. 2008, A&A, 487, 865
Rossetti, A., Mantovani, F., Dallacasa, D., et al. 2009, A&A, 504, 741
Saikia, D. J. 1999, MNRAS, 302, L60
Saikia, D. J., Swarup, G., & Kodali, P. D. 1985, MNRAS, 216, 385
Saikia, D. J., Singal, A. K., & Cornwell, T. J. 1987, MNRAS, 224, 379
Saikia, D. J., Jeyakumar, S., Wiita, P. J., Sanghera, H. S., & Spencer, R. E. 1995, MNRAS, 276, 1215
Saikia, D. J., Holmes, G. F., Kulkarni, A. R., Salter, C. J., & Garrington, S. T. 1998, MNRAS, 298, 877
Spencer, R. E., Schilizzi, R. T., Fanti, C., et al. 1991, MNRAS, 250, 225
Tabara, H., & Inoue, M. 1980, A&AS, 39, 373
Taylor, G. B. 2000, ApJ, 533, 95
Taylor, G. B., Inoue, M., & Tabara, H. 1992, A&A, 264, 421
Udomprasert, P. S., Taylor, G. B., Pearson, T. J., & Roberts, D. H. 1997, ApJ, 483, L9
van Breugel, W. J. M., Fanti, C., Fanti, R., et al. 1992, A&A, 256, 56
Venturi, T., & Taylor, G. B. 1999, AJ, 118, 1931
Zavala, R. T., & Taylor, G. 2002, ApJ, 566, L9
Zavala, R. T., & Taylor, G. 2003, ApJ, 589, 126
Zavala, R. T., & Taylor, G. 2004, ApJ, 612, 749